

# Efficient Distributed Training via Dual Batch Sizes and Cyclic Progressive Learning

Kuan-Wei Lu, Ding-Yong Hong, Pangfeng Liu, and Jan-Jan Wu

**Abstract**—Distributed machine learning is critical for training deep learning models on large datasets and with numerous parameters. Current research primarily focuses on leveraging additional hardware resources and powerful computing units to accelerate the training process. As a result, larger batch sizes are often employed to speed up training. However, training with large batch sizes can lead to lower accuracy due to poor generalization. To address this issue, we propose the *dual batch size learning* scheme, a distributed training method built on the parameter server framework. This approach maximizes training efficiency by utilizing the largest batch size that the hardware can support while incorporating a smaller batch size to enhance model generalization. By using two different batch sizes simultaneously, this method reduces testing loss and enhances generalization, with minimal extra training time. Additionally, to mitigate the time overhead caused by dual batch size learning, we propose the *cyclic progressive learning* scheme. This technique gradually adjusts image resolution from low to high during training, significantly boosting training speed. By combining cyclic progressive learning with dual batch size learning, our *hybrid* approach improves both model generalization and training efficiency. Experimental results using ResNet-18 show that, compared to conventional training methods, our method can improve accuracy by 3.3% while reducing training time by 10.6% on CIFAR-100, and improve accuracy by 0.1% while reducing training time by 35.7% on ImageNet.

**Index Terms**—deep neural networks, batch sizes, distributed learning, parameter server, progressive learning

## I. INTRODUCTION

DEEP learning has achieved remarkable success in a wide range of applications in recent years. Notably, it has excelled in computer vision tasks, including image classification [1]–[3], object detection [4]–[6], semantic segmentation [7]–[9], and many others.

Despite these advancements, training deep learning models remains computationally intensive due to the large number of parameters and the high computational workload. In addition, hardware architecture imposes inherent limitations on computational power. For example, the number of physical cores limits computational parallelism, while memory capacity limits the maximum amount of data that can be processed simultaneously. Therefore, enlarging the batch size while extending the parallelism to reduce training time has become crucial in deep learning model training.

Kuan-Wei Lu, Ding-Yong Hong, and Jan-Jan Wu are with Institute of Information Science, Academia Sinica, Taipei, Taiwan (e-mail: andylu6046@iis.sinica.edu.tw; wuj@iis.sinica.edu.tw; dyhong@iis.sinica.edu.tw).

Pangfeng Liu is with Department of Computer Science and Information Engineering, National Taiwan University, Taipei, Taiwan (e-mail: pangfeng@csie.ntu.edu.tw).

To overcome hardware memory and computing power limitations, researchers have proposed *distributed learning* [10]–[12]. By integrating multiple processors into a training cluster, both computing power and memory capacity can be significantly expanded beyond the limits of a single processor. In recent works [13]–[15], researchers leveraged large-scale GPU/TPU clusters for distributed training. By aggregating computation across multiple processors, batch sizes can increase from hundreds to thousands, thereby significantly reducing training time.

However, while training with large batch sizes enhances hardware utilization and accelerates the training process, it often leads to lower accuracy and poor generalization. This issue arises because larger batch sizes reduce gradient diversity, leading to models that converge to sharp minima in the loss landscape [16]. Sharp minima correspond to solutions that perform well on training data but generalize poorly to unseen data. Additionally, the reduced noise in large-batch updates weakens the implicit regularization effect that smaller batches provide, which can further contribute to overfitting and decreased generalization ability.

To mitigate the challenges posed by large batch sizes, we propose *dual batch size learning*, a method that trains deep neural networks (DNN) using two batch sizes simultaneously. We use the maximum batch size of the hardware for maximum training efficiency. Additionally, we incorporate a smaller batch size during training to increase gradient diversity, thereby improving the model’s generalization ability. Furthermore, since the data processing speeds for two different batch sizes are different, we must assign the data proportionally to maximize the overall processing speed and adjust their contributions to the global weight update accordingly. Hence, we propose adjusting the contribution ratio based on the amount of data processed in small and large batches. The preceding methods are published in IEEE COMPSAC 2022 [17].

In this article, we further optimize the dual batch size learning method to reduce training time. To achieve this, we propose *cyclic progressive learning*, a scheduling strategy that divides the training process into stages, adjusting the image resolutions from low to high within each stage. By integrating cyclic progressive learning with dual batch size learning, this *hybrid* approach not only enhances model generalization by exposing the models to images of varying sizes, but also reduces training time by leveraging smaller images in each training stage.

The contributions of this paper are as follows:

- We introduce a training strategy that uses two different

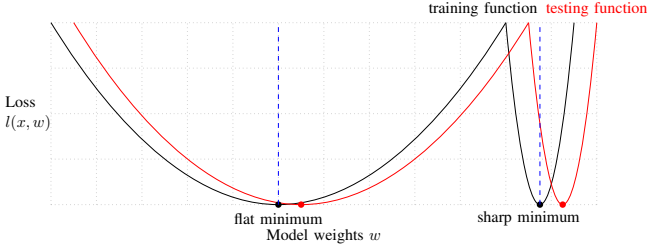


Fig. 1. Illustration of sharp and flat minima in the loss landscape. A sharp minimum leads to higher testing loss, resulting in poor generalization, while a flat minimum causes only a small increase in loss, thereby improving generalization [16].

batch sizes simultaneously to balance training efficiency and accuracy.

- We propose the *model-update factor*, which ensures training contributions from different batch sizes are proportionally integrated into the global parameters based on the amount of data processed.
- We reduce training time through an adaptive learning schedule that adjusts image resolutions and model regularization across training stages.

The remainder of this paper is organized as follows. Section II provides an overview of distributed learning, including how batch size affects training, the training framework, and distributed learning schemes. Section III explains dual batch size learning, while Section IV introduces cyclic progressive learning and the hybrid scheme. Section V presents experimental results to evaluate the effectiveness of our proposed method. Finally, Section VI summarizes the paper.

## II. BACKGROUND

### A. The Effect of Batch Size

The concept of sharp and flat minima is described in [16] and illustrated in Figure 1. A *sharp minimum*  $\hat{w}$  occurs when the loss function increases *rapidly* near  $\hat{w}$ . In contrast, a *flat minimum*  $\bar{w}$  occurs when the loss function increases *slowly* near  $\bar{w}$ .

Batch size plays a crucial role in deep neural network training outcomes [16], [18]–[22]. Training with a large batch size reduces training time but often leads to convergence at a sharp minimum in the loss landscape, resulting in higher testing loss and lower accuracy. This indicates that models trained with larger batch sizes struggle to generalize to unseen data. In contrast, training with a smaller batch size increases training time but is more likely to lead the model toward a flat minimum, yielding lower testing loss and higher accuracy. As a result, models trained with smaller batch sizes generally exhibit stronger generalization and better test performance compared to those using larger batch sizes [23], [24].

### B. Stochastic Gradient Descent

Stochastic gradient descent (SGD) is a standard optimization algorithm that updates model parameters using gradients, as shown in Equation 1. Here,  $n$  is the batch size,  $w_t$  is the model’s weights at iteration  $t$ ,  $\eta$  is the learning rate,  $B$  is a

mini-batch (of size  $n$ ) sampled from the labeled training set  $X$ , and  $l$  is the loss function.

$$\begin{aligned} w_{t+1} &= w_t - \eta g \\ &= w_t - \eta \left( \frac{1}{n} \sum_{x \in B} \nabla l(x, w_t) \right) \end{aligned} \quad (1)$$

We assume that the gradient  $g$  follows a distribution with mean  $\mu_g$  and variance  $\sigma_g^2$ . We randomly select  $N$  samples from  $g$  with replacement and compute their average. According to the *central limit theorem*, the sample average  $\bar{g}$  follows a normal distribution. Thus,  $\bar{g}$  follows a normal distribution with mean  $\mu_{\bar{g}} \approx \mu_g$  and variance  $\sigma_{\bar{g}}^2 \approx \frac{\sigma_g^2}{N}$ . When the batch size  $N$  increases, the sample mean is more likely to approximate the population mean, as variance decreases with increasing  $N$ . Conversely, with a smaller batch size, the sample mean is more prone to deviation from the population mean.

The batch size directly influences the training behavior of the model. Gradients from large batch sizes exhibit slight deviations because they are more stable, making it harder for gradient descent to escape from sharp minima. In contrast, smaller batch sizes have larger deviations, facilitating escape from sharp minima.

Figure 1 illustrates the loss (y-axis) as a function of model weights (x-axis). The black line, *training loss function*, indicates the loss computed using only the training data. The red line, *testing loss function*, shows the loss computed using the test data that were not part of the training set.

In Figure 1, we assume that increasing the amount of input data causes the loss function to transition from the black line (training function) to the red line (testing function). If the model converges to a sharp minimum on the black line, the loss increases significantly when shifting to the red line. In contrast, if the model converges to a flat minimum, the loss increases only slightly when shifting to the red line. Since small-batch training typically leads to a flat minimum while large-batch training leads to a sharp minimum, small-batch training generally results in lower testing loss than large-batch training.

### C. Parameter Server Framework

The parameter server framework [25]–[29] is a widely used method for centralized distributed training. A parameter server system consists of a server and multiple workers, as illustrated in Figure 2. The server maintains the global model, updates parameters, and coordinates the workers. The worker is responsible for the training computation. A worker receives parameters from the server, trains the model, and sends the results back to the server.

In a parameter server framework, model training proceeds as follows. At the start of each iteration, each worker requests (or *pulls*) the global model from the server. The workers then replace their local models with the received global model. Next, the workers train the model and update their parameters locally. Once training is complete, the workers send (or *push*) the updated parameters back to the server, which then updates the global model. This cycle repeats until the model converges or reaches a predetermined number of iterations.

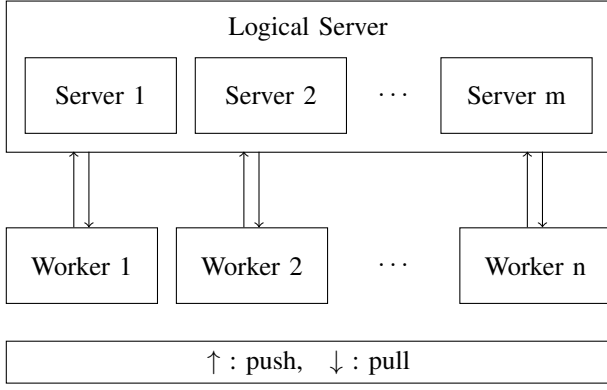


Fig. 2. Architecture of the parameter server framework for distributed deep learning. The server maintains the global parameters, while multiple workers perform local training and send back the updated parameters.

#### D. Synchronization Strategy

Researchers have proposed several synchronization strategies to achieve both data consistency and high performance in distributed learning across multiple machines [30]–[38]. These strategies can be broadly classified into three categories: bulk synchronous parallel (BSP), asynchronous parallel (ASP), and stale synchronous parallel (SSP).

The *bulk synchronous parallel* (BSP) [30], [31] is a commonly used synchronization scheme that operates with a *barrier*. At the start of each iteration, the server informs the workers to pull the global model. Each worker then trains the model and computes the gradients independently. After training, the worker pushes the updated parameters back to the server and waits for synchronization. Once the server receives the parameters from all workers, it updates the global model and notifies all workers to begin the next iteration. The advantage of BSP is that all workers have the same local model at the start of each iteration, ensuring consistency. However, the disadvantage is that all workers must wait for the slowest one to push its parameters, which can result in longer training time.

The *asynchronous parallel* (ASP) [32]–[34] is a synchronization scheme that operates without a barrier. Unlike BSP, where the server waits for all workers to push their gradients before proceeding, each worker in an ASP model *independently* pulls the global model from the server and updates the model without waiting for other workers. Thus, when a worker computes gradients and pushes them back, the server immediately updates the model without synchronization. This results in shorter training time since there is no waiting. However, the inconsistency between local models can lead to difficulties in convergence.

The *stale synchronous parallel* (SSP) [35], [36] is a flexible synchronization scheme that lies between ASP and BSP. SSP introduces a hyper-parameter, the *staleness threshold*  $s$ , which limits the iteration gap between the fastest and slowest workers. When the gap is within  $s$ , the workers behave like an ASP model, independently communicating with the server. If the gap reaches  $s$ , the server suspends the fastest worker until the slowest worker catches up and pushes its parameters.

BSP and ASP can be considered as special cases of SSP. SSP becomes ASP when  $s$  is infinite, allowing workers to proceed without synchronization, and SSP becomes BSP when  $s$  is 0, requiring workers to synchronize at every iteration.

### III. DUAL BATCH SIZE LEARNING

#### A. Overview

We propose the *dual batch size learning* scheme, which employs two batch sizes simultaneously during model training on the parameter server. This approach reduces the testing loss, thereby improving accuracy. The dual batch sizes are chosen to leverage the stability of gradient descent obtained from the large batch size and the strong generalization ability derived from the small batch size. Additionally, we adopt *asynchronous parallel* training due to the different training speeds of the two batch sizes. If a synchronous learning scheme is used, the smaller batch size would slow down the training process, thereby reducing overall training efficiency.

The dual batch size learning scheme addresses three issues. First, it predicts the training time for different batch sizes in order to allocate the input data appropriately between them. Second, it selects optimal batch sizes and allocates data to each batch to ensure balanced training times. Lastly, it evaluates the relative contribution of each batch size and integrates these contributions into the global model during the weight update phase.

#### B. Training Time Prediction

The dual batch size learning scheme requires an accurate prediction of training time as a function of batch size. Once the training time can be predicted, it enables the selection of appropriate batch sizes for the training process. Thus, an accurate training time prediction model is essential.

The training time depends on the batch size, which is determined by the amount of training data per batch and the GPU hardware. Additionally, the total training time is the product of the training time per batch and the total number of batches. We assume the training time is a linear function of the batch size  $x$ , denoted as  $ax + b$ . Let the total amount of data be  $d$ ; the number of batches required for training would then be  $\lceil \frac{d}{x} \rceil$ . Thus, the total training time  $t$  is given by Equation 2.

$$t = (ax + b) \cdot \lceil \frac{d}{x} \rceil \quad (2)$$

We conduct experiments to validate the correctness of Equation 2. For the experiments, we choose two widely used machine learning frameworks: PyTorch [39] and TensorFlow [40]. The training dataset consists of 50,000  $32 \times 32$  images, and we use an NVIDIA GTX 1080 GPU to train a ResNet-18 model. We train the model with batch sizes ranging from 1 to 500.

We first validate the assumption that the training time per batch is a linear function of the batch size. Figure 3 shows the training time per batch for different batch sizes in both PyTorch and TensorFlow. Then we can estimate  $a$  and  $b$  through linear regression.

Figure 3 shows that TensorFlow’s training time is more predictable than PyTorch’s. The unpredictability of PyTorch’s

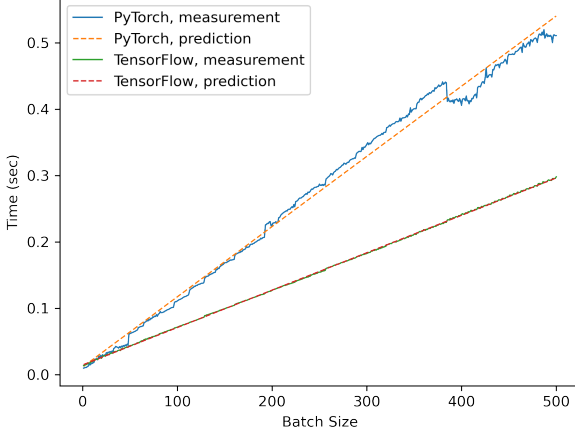


Fig. 3. Training time per batch for different batch sizes in PyTorch and TensorFlow. The results highlight the linear relationship between batch size and training time.

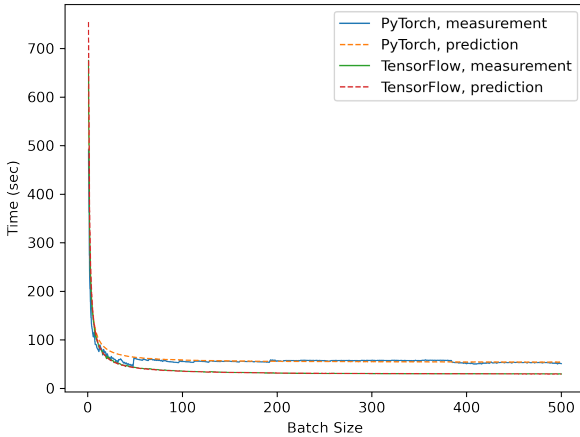


Fig. 4. Training time per epoch for different batch sizes. Larger batch sizes improve GPU utilization and reduce training time, as validated by experimental results.

training time may arise from the back-end implementation of the framework. PyTorch checks the batch size and calls different NVIDIA cuDNN [41] kernel libraries for accordingly. In contrast, TensorFlow is oblivious to the batch size and determines the back-end implementation based on operation parameters and hardware information. For the sake of predictability, we use TensorFlow to conduct our experiments.

Figure 4 shows the predicted and actual training time for an epoch in both PyTorch and TensorFlow under different batch sizes. The results show that training time decreases as batch size increases, since larger batch sizes make more efficient use of GPU resources. Additionally, we observe that Equation 2 accurately predicts the training time for TensorFlow across all batch sizes.

### C. Batch Size and Data Amount

The dual batch size learning scheme employs two batch sizes, denoted by  $B_S$  (small batch size) and  $B_L$  (large batch size), where  $B_S < B_L$ . When using  $B_L$  on all GPUs, the training time  $t$  will be minimized. However, if  $B_S$  is used on some GPUs, the training time increases. In the following, we allocate  $\hat{t} = kt > t$  time for training and call  $k > 1$  the *extra training time ratio*. We aim to explore the trade-offs by introducing this extra training time ratio.

Load balancing is an essential issue in dual batch size learning. If the same amount of data is allocated to each worker regardless of batch size, the training time will vary across batch sizes, leading to the *straggler problem*. In this scenario, slower workers take significantly longer to complete their tasks, causing delays in the overall training process. To address this, we allocate  $d_S$  data to each worker with batch size  $B_S$  and  $d_L$  data to each worker with batch size  $B_L$ , ensuring that the workload is evenly distributed across all workers.

We first simplify Equation 2 into Equation 3.

$$t \approx \left(a + \frac{b}{x}\right) \cdot d \quad (3)$$

We calculate the time required when using only the large batch size  $B_L$  on all  $n$  workers. Given that the total data amount is  $d$ , the data amount per worker can be denoted as  $\frac{d}{n}$ . From Equation 3 the time can be expressed as  $\left(a + \frac{b}{B_L}\right) \frac{d}{n}$ .

Suppose we want to use  $n_L$  workers with large batch size  $B_L$  and  $n_S$  workers with small batch size  $B_S$ . We need an even workload distribution between these two different batch sizes. Therefore, the training time for both small and large batches should be  $k\left(a + \frac{b}{B_L}\right) \frac{d}{n}$ , which represents a time that is  $k$  times longer than when using only the large batch size  $B_L$  on all  $n$  workers, as shown in Equations 4 and 5.

$$k\left(a + \frac{b}{B_L}\right) \frac{d}{n} = \left(a + \frac{b}{B_L}\right) d_L \quad (4)$$

$$= \left(a + \frac{b}{B_S}\right) d_S \quad (5)$$

From Equation 4, we can easily derive that  $d_L = k \cdot \frac{d}{n}$ . Additionally,  $d_S$  can be obtained from Equation 6 once  $d_L$  is determined.

$$d = n_L d_L + n_S d_S \quad (6)$$

By combining Equations 4 and 5, we derive Equation 7. Through transposing terms, Equation 7 can be transformed into Equation 8.

$$\left(a + \frac{b}{B_L}\right) d_L = \left(a + \frac{b}{B_S}\right) d_S \quad (7)$$

$$B_S = \frac{b}{\left(a + \frac{b}{B_L}\right) \frac{d_L}{d_S} - a} \quad (8)$$

Finally, since  $B_L$ ,  $d_L$ , and  $d_S$  are given, we can use Equation 8 to determine  $B_S$ . Here, the parameters  $a$  and  $b$  are obtained from Section III-B via linear regression. Using this approach, the optimal  $B_S$  varies depending on the hardware configuration.

#### D. Model-Update Factor

Since different workers process different amounts of data, the importance of each worker's contribution should be different. Workers using the large batch size  $B_L$  handle a more significant amount of data  $d_L$ , and thus their parameters are more critical. In contrast, workers using the small batch size  $B_S$  process less data  $d_S$ , and their parameters are less critical.

During the model update phase, we adjust the contributions of different batch size workers into the global parameters, taking into account the amounts of data processed. We set the model-update factor for workers handling the large batch size  $B_L$  to be 1. For workers handling the small batch size  $B_S$ , we propose two different schemes of model-update factors. The first model-update factor is  $\frac{d_S}{d_L}$ , which reflects the amount of data processed by the small-batch and large-batch workers. The second model-update factor is  $\sqrt{\frac{d_S}{d_L}}$ . According to the introduction of the batch size effect on the gradient in Section II-A, the amount of data is proportional to the batch size, which in turn is proportional to the variation of the gradient. The standard deviation of the gradient, which is the square root of the variance, should reflect the importance of the weights updated by the small-batch workers. A similar argument can be found in the work of Smith et al. [14]. In summary, when a worker updates the global model, its contribution is multiplied by the model-update factor, which depends on the amount of data processed by the worker. Both schemes balance the contributions from small and large batch workers.

### IV. PROGRESSIVE LEARNING

#### A. Cyclic Progressive Learning

To further reduce training time and enhance the model's generalization ability in dual batch size learning, we propose the *cyclic progressive learning* scheme, which is an improved version of progressive learning [42]. This scheme provides two advantages based on varying image resolutions: (1) reduced training time when using low-resolution images, and (2) enhanced accuracy when using high-resolution images. Additionally, exposing the model to a broader range of image resolutions helps mitigate overfitting, thereby improving model generalization.

The motivation behind cyclic progressive learning comes from prior research on *progressive resizing* [43] and *adaptive regularization* [42]. Progressive resizing starts with training on images compressed to low resolution and then gradually increases the image resolution. The underlying idea is that learning basic features does not require high-resolution details, while later stages benefit from higher-resolution images to capture finer variations. Adaptive regularization, on the other hand, dynamically adjusts the regularization strength based on image resolution, addressing the potential accuracy degradation caused by imbalanced regularization across different image resolutions.

The integration of progressive learning with dual batch size learning involves addressing two challenges. First, progressive learning typically uses a fixed batch size, which is determined based on high-resolution images to avoid exceeding the

TABLE I  
COMPARISON OF THE PROPOSED TRAINING SCHEMES WITH TWO STAGES AND TWO SUB-STAGES. THE MAIN DIFFERENCES INCLUDE LEARNING RATE  $\eta$ , BATCH SIZE  $B$ , IMAGE RESOLUTION  $r$ , AND DROPOUT RATE  $d$ .

scheme	stage sub-stage	1		2	
		1	2	1	2
dual batch size learning	LR BS resolution dropout	$\eta_1$		$\eta_2$	
		$B_{S_2}/B_{L_2}$		$B_{S_1}/B_{L_1}$	
		$r_2$		$r_1$	
		$d_2$		$d_1$	
cyclic progressive learning	LR BS resolution dropout	$B_1$ $r_1$ $d_1$	$\eta_1$ $B_2$ $r_2$ $d_2$	$B_1$ $r_1$ $d_1$	$\eta_2$ $B_2$ $r_2$ $d_2$
hybrid scheme	LR BS resolution dropout	$B_{S_1}/B_{L_1}$ $r_1$ $d_1$	$\eta_1$ $B_{S_2}/B_{L_2}$ $r_2$ $d_2$	$B_{S_1}/B_{L_1}$ $r_1$ $d_1$	$\eta_2$ $B_{S_2}/B_{L_2}$ $r_2$ $d_2$

GPU's memory capacity. This fixed batch size leads to GPU underutilization during training with low-resolution images. Second, high-resolution images are introduced in the later phases of training when the learning rate is already low. While high-resolution images improve model performance, the low learning rate limits the extent of weight adjustments (as shown in Equation 1).

To overcome these issues, the cyclic progressive learning scheme introduces two innovative features: adaptive batch sizes and learning rates. To maximize GPU utilization, we dynamically adjust batch sizes based on image resolutions. The batch size is increased when training with low-resolution images, ensuring better utilization of GPU resources. Furthermore, instead of using low learning rates for high-resolution images, we train across all image resolutions using *all* predefined learning rates. More specifically, we divide the training process (and the learning rate schedule) into multiple stages. In each stage, the model is trained with images of progressively increasing resolutions, allowing it to adapt gradually to more complex features. This strategy ensures that each image resolution contributes effectively to weight updates with appropriate learning rates.

Table I illustrates an example of cyclic progressive learning (third row). In this example, the training process is first divided into two stages with learning rates  $\eta_1$  and  $\eta_2$ , respectively. In each stage, the image resolution  $r$  and dropout rate  $d$  increase gradually every few epochs, while batch sizes  $B$  are adjusted according to the image resolutions.

#### B. Hybrid Scheme

We integrate cyclic progressive learning with the dual batch size learning scheme, which we refer to as the *hybrid scheme*. The hybrid scheme addresses the increased training time caused by using small batches. While dual batch size learning naturally extends training time, incorporating cyclic progressive learning helps mitigate this by leveraging image resolution resizing, thereby improving overall training efficiency despite the use of smaller batches. Furthermore, by combining multiple batch sizes and image resolutions, the hybrid scheme enhances the model's generalization ability.

Table I illustrates an example of the hybrid scheme (fourth row). In contrast to dual batch size learning, the hybrid scheme trains the model at each stage with dynamically adjusted image resolutions, and the batch sizes are automatically adapted as well according to these resolutions. Unlike pure cyclic progressive learning, the hybrid scheme extends the batch sizes within each stage from a single size to two different batch sizes, thus leveraging the benefits of both.

## V. EXPERIMENTS

In this section, we first evaluate the effectiveness of dual batch size learning. Next, we assess the performance of combining the dual batch size learning scheme with cyclic progressive learning. Then, we analyze the accuracy of the method that automatically determines the maximum batch size for a given GPU.

### A. Training with Dual Batch Size Learning

1) *Experimental Setup*: We use the CIFAR-100 [44] dataset for the image classification task. CIFAR-100 consists of 60,000  $32 \times 32$  color images in 100 classes, with each class containing 500 training images and 100 testing images. In total, the dataset includes 50,000 training images and 10,000 testing images.

ResNet-18 [3] serves as our evaluation model. This deep neural network consists of eighteen convolutional layers and a fully connected layer. ResNet-18 uses residual learning to enhance model depth and improve accuracy.

We train ResNet-18 with TensorFlow [40] version 2.6 on the parameter server framework. The parameter server framework consists of one server and four workers, forming a GPU cluster. Each machine is equipped with an Intel Xeon E5-1630 v3 CPU, 64GB RAM, and an NVIDIA GeForce GTX 1080 GPU, running Ubuntu 18.04 LTS Linux. The devices are connected by 1Gbps Ethernet.

2) *Evaluation of Model-Update Factor*: Since small-batch workers train on a smaller amount of data than large-batch workers, it seems reasonable that the training results from small-batch workers should have *less* influence when updating the global model. To verify this, we compare the accuracy of using the two model-update factors ( $\frac{d_S}{d_L}$  and  $\sqrt{\frac{d_S}{d_L}}$ ) with the case where no model-update factor is applied. In this experiment, we set the extra training time ratio  $k$  to 1.1. The lower part of Table III lists the training configuration, including batch sizes and data amounts for the workers.

Table II presents the performance results, and Figures 5 and 6 respectively illustrate the testing loss and testing accuracy throughout the training process. The results indicate that using the model-update factor  $\frac{d_S}{d_L}$  improves accuracy in all cases, achieving up to 0.9% improvement compared to training without it. In contrast, the model-update factor  $\sqrt{\frac{d_S}{d_L}}$  does not perform as well as  $\frac{d_S}{d_L}$ . Although  $\sqrt{\frac{d_S}{d_L}}$  yields a 0.4% improvement over  $\frac{d_S}{d_L}$  when training with two small-batch workers, it performs worse in the other two cases. Since  $\frac{d_S}{d_L}$  consistently outperforms the training without the model-update factor in the experiments, we conclude that applying the model-update

TABLE II  
IMPACT OF THE MODEL-UPDATE FACTOR ON TRAINING RESULTS.

$n_S / n_L$	model-update factor	value	$B_S$	$d_S$	testing loss	testing accuracy	accuracy improvement
1 / 3	$\frac{d_S}{d_L}$	0.636	38	8750	1.193	68.5%	0.5%
	$\sqrt{\frac{d_S}{d_L}}$	0.797			1.179	67.8%	-0.2%
	-	-			1.187	68.0%	-
2 / 2	$\frac{d_S}{d_L}$	0.818	87	11250	1.250	70.5%	0.3%
	$\sqrt{\frac{d_S}{d_L}}$	0.904			1.270	70.9%	0.7%
	-	-			1.295	70.2%	-
3 / 1	$\frac{d_S}{d_L}$	0.879	127	12083	1.327	70.7%	0.9%
	$\sqrt{\frac{d_S}{d_L}}$	0.938			1.383	70.4%	0.6%
	-	-			1.411	69.8%	-

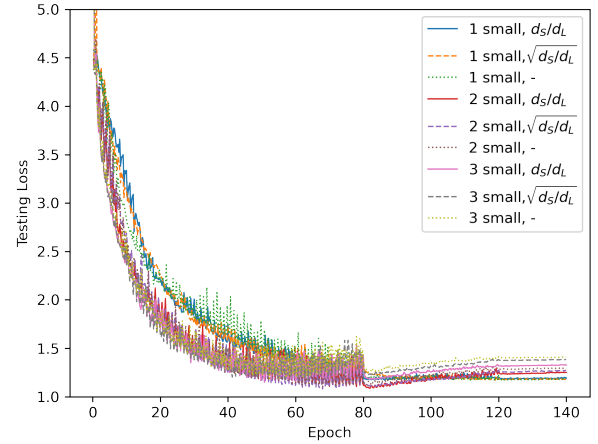


Fig. 5. Comparison of testing loss under three conditions: with  $\frac{d_S}{d_L}$ , with  $\sqrt{\frac{d_S}{d_L}}$ , and without a model-update factor.

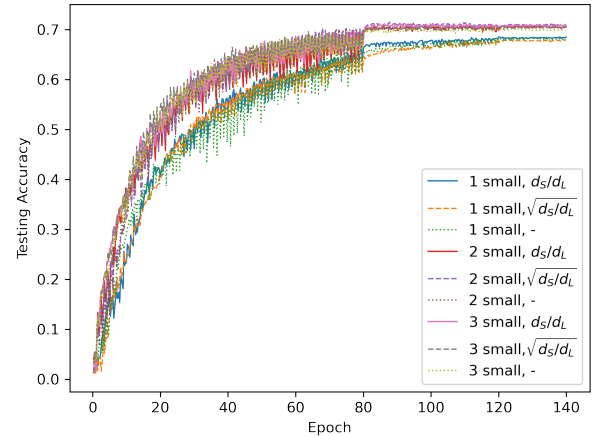


Fig. 6. Comparison of testing accuracy under three conditions: with  $\frac{d_S}{d_L}$ , with  $\sqrt{\frac{d_S}{d_L}}$ , and without a model-update factor.

factor enhances training effectiveness. Therefore, we will use the model-update factor  $\frac{d_S}{d_L}$  in the remaining experiments.

3) *Evaluation of Numbers of Small-batch Workers*: Despite the fact that small-batch workers can achieve lower loss, the number of such workers must be sufficient to increase the



TABLE III

TRAINING PARAMETERS FOR DIFFERENT NUMBERS OF SMALL-BATCH WORKERS, UNDER EXTRA TRAINING TIME RATIOS OF 1.05 AND 1.1.

$k$	$(n_S, n_L)$	$B_S$	$d_S$	$B_L$	$d_L$	$\frac{d_S}{d_L}$
1.05	(1, 3)	83	10625			0.810
	(2, 2)	154	11875	500	13125	0.905
	(3, 1)	205	12291			0.936
	(4, 0)	242	12500	-	-	-
1.1	(1, 3)	38	8750			0.636
	(2, 2)	87	11250	500	13750	0.818
	(3, 1)	127	12083			0.879
	(4, 0)	160	12500	-	-	-

final accuracy. According to Equation 8, reducing the number of small-batch workers ( $n_S$ ) decreases the optimal small-batch size ( $B_S$ ). In addition, according to Equation 6, the amount of data allocated to these workers ( $d_S$ ) also decreases. However, if the number of small-batch workers is small, they train much less data than large-batch workers. As a result, insufficient small-batch training data leads to minor accuracy improvement.

We conduct experiments to demonstrate the importance of having a sufficient number of small-batch workers. In these experiments, we set the large-batch size ( $B_L$ ) as high as possible to maximize GPU utilization and reduce training time. Specifically, we set  $B_L$  to 500, which is close to the maximum batch size allowed on the GPU, as larger values cause TensorFlow to trigger memory warnings. Hence, our baseline for comparison is when all workers train the models with a batch size of 500. We use four workers to train the model for 140 epochs. The initial learning rate is 0.1, and it decreases by a factor of 5 at the 80th and 120th epochs.

For comparison purposes, the baseline method is enhanced using the gradual warm-up strategy [13] to improve accuracy. We start from a learning rate of  $\frac{0.1}{5}$  and increase it until it reaches 0.1 after five epochs. The baseline converges at a loss of 1.429 and an accuracy of 67.8%.

**$k = 1.05$ .** We first evaluate the performance when  $k$  is 1.05. We set  $B_L$  to 500, which is the same as the baseline's batch size. Given that CIFAR-100 has 50,000 training data, we can derive  $d_L$  as 13,125 according to Equation 4. We vary the number of small-batch workers ( $n_S$ ) from 1 to 4. Correspondingly, the number of large-batch workers ( $n_L$ ) changes from 3 to 0. Using Equations 6 and 8, we compute  $d_S$  and  $B_S$  for each combination of  $n_S$  and  $n_L$ , since we have determined  $d_L$  and  $B_L$ . In addition, we also calculate the model-update factor ( $\frac{d_S}{d_L}$ ). The upper part of Table III lists these parameters for the training process.

Accurate prediction is essential for the effectiveness of our dual batch size learning. Hence, we check how accurately Equation 2 can predict the training time as a function of the batch size and corresponding data amount. We measure the training time by averaging five runs and compare it with the predicted time from Equations 4 and 5. The upper part of Table IV shows the measured training time, predicted time, and the relative error across different batch sizes and data amounts. We observe that the maximum relative error is +3.5%, occur-

TABLE IV

THE MEASURED TIME, PREDICTED TIME, AND RELATIVE ERROR FOR DIFFERENT NUMBERS OF SMALL-BATCH WORKERS, UNDER EXTRA TRAINING TIME RATIOS OF 1.05 AND 1.1.

extra training time ratio	batch size	data amount	measured time	predicted time	relative error
1.05	500	13125	8.098	7.821	+3.5%
	83	10625	7.989	7.985	+0.1%
	154	11875	7.615	7.816	-2.6%
	205	12291	7.622	7.792	-2.2%
	242	12500	7.610	7.757	-1.9%
1.1	500	13750	8.182	8.193	-0.1%
	38	8750	8.183	8.398	-2.5%
	87	11250	8.141	8.338	-2.4%
	127	12083	8.220	8.163	+0.7%
	160	12500	8.222	8.135	+1.0%

TABLE V

TRAINING RESULTS FOR DIFFERENT NUMBERS OF SMALL-BATCH WORKERS, UNDER EXTRA TRAINING TIME RATIOS OF 1.05 AND 1.1.

$B_L = 500$ 4 workers	$(n_S, n_L)$	$B_S$	loss	accuracy	accuracy improvement
$k = 1$	(0, 4)	-	1.429	67.8%	-
$k = 1.05$	(1, 3)	83	1.246	67.9%	0.1%
	(2, 2)	154	1.290	70.1%	2.3%
	(3, 1)	205	1.372	70.6%	2.8%
	(4, 0)	242	1.399	70.1%	2.3%
$k = 1.1$	(1, 3)	38	1.193	68.5%	0.7%
	(2, 2)	87	1.250	70.5%	2.7%
	(3, 1)	127	1.327	70.7%	2.9%
	(4, 0)	160	1.415	70.5%	2.7%

ring at the batch size of 500 and the corresponding data amount of 13,125. This indicates that our prediction is accurate enough for the dual batch size learning to be feasible.

After verifying the accurate prediction of training time for different batch sizes, we proceed with training using different numbers of small-batch workers. The third row of Table V lists the final testing loss and accuracy for all combinations of batch sizes for  $k = 1.05$ ; Figures 7 and 8 show the testing loss and accuracy of the training process. We observe that when one small-batch worker and three large-batch workers are used, we achieve the lowest loss (1.246) among all combinations, and it is 0.183 lower than the baseline method. However, the accuracy of using only *one* small-batch worker is only 0.1% better than the baseline. In contrast, using *three* small-batch workers and one large-batch worker results in a higher loss (1.372), which is worse than using just one small-batch worker. Nevertheless, it achieves the highest accuracy of 70.6%, 2.8% higher than the baseline, and has the best accuracy among all combinations.

The experimental results support our claim. Despite the fact that a worker with a small batch size can achieve low training loss, the number of such workers must be sufficient to increase the final accuracy. Using only one small-batch worker during training will severely limit the amount of data trained by the small batches. In this experiment, if we use only one worker with a small batch size, it trains only 21% of the total data.

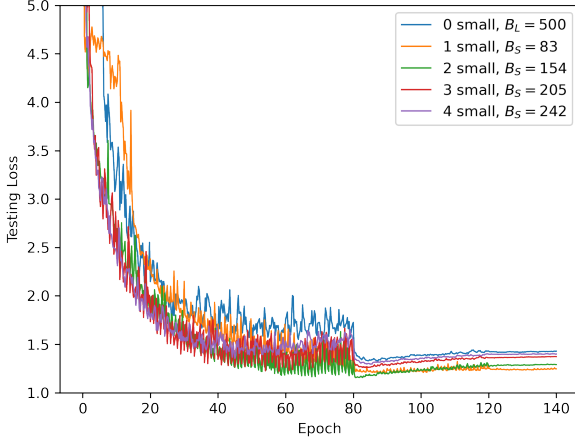


Fig. 7. Effect of different numbers of small-batch workers on testing loss when  $k = 1.05$ .

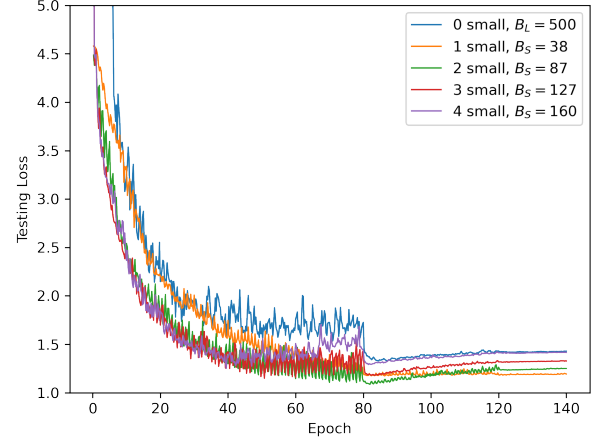


Fig. 9. Effect of different numbers of small-batch workers on testing loss when  $k = 1.1$ .

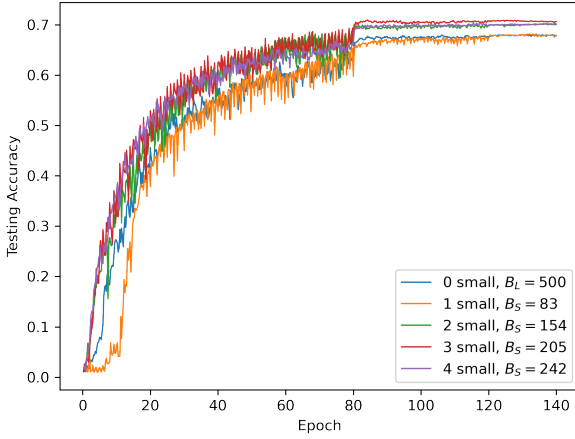


Fig. 8. Effect of different numbers of small-batch workers on testing accuracy when  $k = 1.05$ .

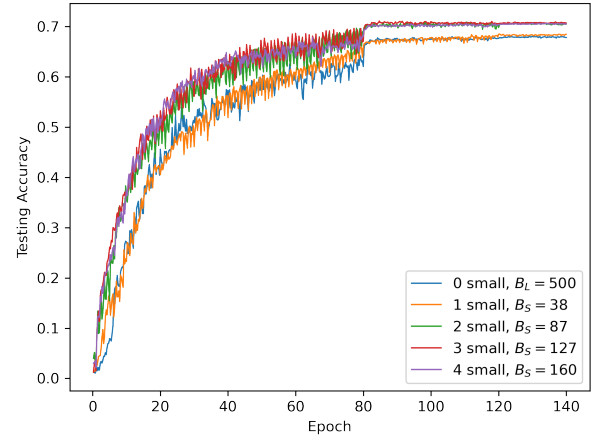


Fig. 10. Effect of different numbers of small-batch workers on testing accuracy when  $k = 1.1$ .

Consequently, even though the loss is minimized, the accuracy is still not the best. In contrast, using three small-batch workers provides 74% of the entire data for the small batches. Although the loss is not the lowest, this setting achieves the highest accuracy among all configurations.

**$k = 1.1$ .** Next, to further validate our claim, we conduct another set of experiments with a different extra training time ratio,  $k = 1.1$ . The training parameters are listed in the lower part of Table III.

Once again, we evaluate the accuracy of Equation 2 for  $k = 1.1$ . The lower part of Table IV shows the timing results and relative error across different batch sizes and data amounts. The results indicate that the maximum relative error is -2.5%, occurring at a batch size of 38 and a corresponding data amount of 8,750. Thus, the prediction is sufficiently accurate.

Figures 9 and 10 illustrate the testing loss and accuracy during the training process, while the fourth row of Table V provides the final loss and accuracy for all combinations of small and large batch sizes. We have a similar observation

that the training with only one small-batch worker achieves the lowest loss but shows only slight accuracy improvement over the baseline as it processes only 18% of the total data. In contrast, training with three small-batch workers achieves the highest accuracy of 70.7%, since these workers process 72% of the entire dataset.

After conducting these two experiments with different  $k$  values, we conclude that insufficient data for small-batch training leads to insignificant accuracy improvement. Therefore, appropriately increasing the number of small-batch workers in our scheme can help improve accuracy.

### B. Training with Hybrid Scheme

In this section, we compare the performance of the hybrid scheme with the dual batch size learning scheme.

1) *Experimental Setup:* We use ResNet-18 as the test model and train the model using TensorFlow version 2.13. In addition to training on the CIFAR-100 dataset, we also evaluate the



TABLE VI  
BATCH SIZE AND DATA AMOUNT FOR CIFAR-100 AND IMAGENET  
TRAINING WITH FOUR WORKERS.

CIFAR-100 $k = 1.05$	image resolution = 24 / 32			
	$B_S$	$B_L$	$d_S$	$d_L$
$n_S = 0$	-	-	-	12500
$n_S = 1$	130 / 102	600 / 560	10625	13125
$n_S = 2$	230 / 185		11875	
$n_S = 3$	294 / 243		12292	
$n_S = 4$	340 / 286	-	12500	-

ImageNet $k = 1.05$	image resolution = 160 / 224 / 288			
	$B_S$	$B_L$	$d_S$	$d_L$
$n_S = 0$	-	-	-	320292
$n_S = 1$	156 / 112 / 67	2330 / 1110 / 740	272249	336306
$n_S = 2$	322 / 222 / 135		304278	
$n_S = 3$	464 / 310 / 190		314954	
$n_S = 4$	587 / 383 / 236	-	320292	-

TABLE VII  
TRAINING CONFIGURATION FOR RESNET-18 ON CIFAR-100.

stage		1		2		3	
sub-stage		1	2	1	2	1	2
dual batch size learning	epoch	1-80		81-120		121-140	
	LR	0.2		0.02		0.002	
	$B_S$			$B_{S_2}$			
	$B_L$			560			
	resolution			32			
				0.2			
hybrid scheme	epoch	1-40	41-80	81-100	101-120	121-130	131-140
	LR	0.2		0.02		0.002	
	$B_S$	$B_{S_1}$	$B_{S_2}$	$B_{S_1}$	$B_{S_2}$	$B_{S_1}$	$B_{S_2}$
	$B_L$	600	560	600	560	600	560
	resolution	24	32	24	32	24	32
		0.1	0.2	0.1	0.2	0.1	0.2

training performance on ImageNet [45], a large image classification dataset that includes 1,000 classes, approximately 1.3 million training images, and 50,000 validation images. We set the model-update factor to  $\frac{d_S}{d_L}$  and the extra training time ratio to 1.05. Table VI lists the training parameters for CIFAR-100 and ImageNet, derived using the formulas in Section III. For the hybrid scheme, the training process is divided into stages. For example, the small batch sizes are 130 and 102 for the two sub-stages for CIFAR-100 when  $n_S = 1$ . In the following experiments, we use *hybrid* and *DBSL* to denote the hybrid and dual batch size learning schemes, respectively.

2) *CIFAR-100*: The experiment uses a parameter server framework consisting of one server and four workers, with each node equipped with an Intel Xeon E5-1630 v3 CPU, 64GB RAM, and an NVIDIA GeForce GTX 1080 GPU. We train the model for 140 epochs. For the hybrid scheme, we split the training into three stages, comprising 80, 40, and 20 epochs, respectively. In each stage, we evenly divide the training epochs into two sub-stages, which train with image resolutions of  $24 \times 24$  and  $32 \times 32$  pixels, respectively. Table VII shows the detailed training parameters.

Figures 11 and 12 show the testing loss and accuracy for the training process of CIFAR-100, while Table VIII lists the final training results for all worker combinations. The results indicate that, compared to using the dual batch size learning scheme only, the hybrid scheme achieves better testing accuracy in all cases. Moreover, the hybrid scheme

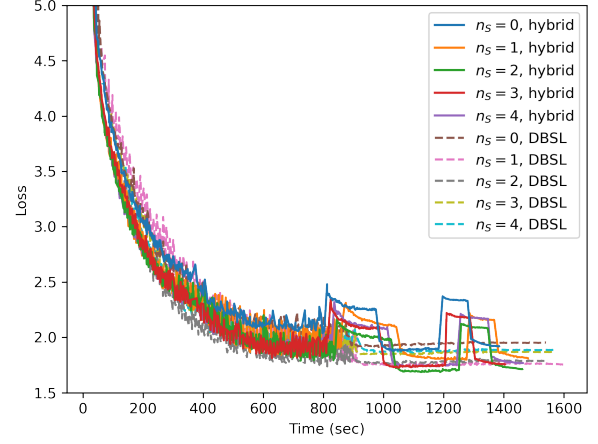


Fig. 11. Validation loss for ResNet-18 trained on CIFAR-100 with different learning schemes.

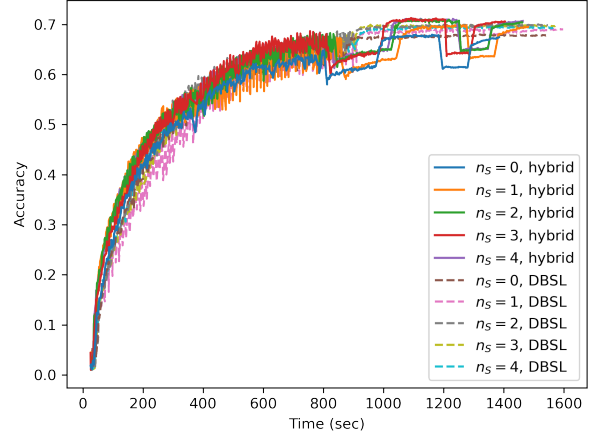


Fig. 12. Validation accuracy for ResNet-18 trained on CIFAR-100 with different learning schemes.

achieves 11.1% training time reduction, where dual batch size learning takes 1,541 seconds to train the model but the hybrid scheme requires only 1,385 seconds. The reduction in training time is due to training with lower-resolution images ( $24 \times 24$ ), and the improvement of accuracy can be attributed to training with images of multiple resolutions, thereby enhancing model generalization.

3) *ImageNet*: Since ImageNet images have higher resolutions than those in CIFAR-100, we use more powerful machines to meet the increased memory and computational demands for ImageNet. We use a setup consisting of one server and four worker nodes, each equipped with an Intel Core i9-12900K CPU, 128GB RAM, and one NVIDIA RTX 3090 GPU. We train the ResNet-18 model for 105 epochs. Due to the higher image resolution in ImageNet, we divide the training process into three stages, each comprising three sub-stages that handle image resolutions of 160, 224, and 288, respectively. To further increase the maximum batch

TABLE VIII  
TRAINING RESULTS FOR RESNET-18 ON CIFAR-100.

$k = 1.05$ 4 workers		loss	accuracy	accuracy improvement
dual batch size learning	$n_s = 0$	1.948	68.0%	0.0%
	$n_s = 1$	1.755	69.1%	1.1%
	$n_s = 2$	1.787	70.0%	2.0%
	$n_s = 3$	1.854	70.0%	2.0%
	$n_s = 4$	1.875	69.8%	1.8%
hybrid scheme	$n_s = 0$	1.893	68.0%	-
	$n_s = 1$	1.805	69.9%	1.9%
	$n_s = 2$	1.691	71.0%	3.0%
	$n_s = 3$	1.729	71.3%	3.3%
	$n_s = 4$	1.735	71.2%	3.2%

TABLE IX  
TRAINING CONFIGURATION FOR RESNET-18 ON IMAGENET.

stage sub-stage		1	1 2	3	1	2 2	3	1	3 2	3
dual batch size learning	epoch	1-60			61-90			91-105		
	LR	0.2			0.02			0.002		
	$B_S$				$B_{S_3}$					
	$B_L$				740					
	resolution dropout				288			0.3		
hybrid scheme	epoch	1-20	21-40	41-60	61-70	71-80	81-90	91-95	96-100	101-105
	LR	0.2			0.02			0.002		
	$B_S$	$B_{S_1}$	$B_{S_2}$	$B_{S_3}$	$B_{S_1}$	$B_{S_2}$	$B_{S_3}$	$B_{S_1}$	$B_{S_2}$	$B_{S_3}$
	$B_L$	2330	1110	740	2330	1110	740	2330	1110	740
	resolution dropout	160	224	288	160	224	288	160	224	288

TABLE X  
TRAINING RESULTS FOR RESNET-18 ON IMAGENET.

$k = 1.05$ 4 workers		loss	accuracy	accuracy improvement
dual batch size learning	$n_s = 0$	1.874	65.9%	0.8%
	$n_s = 1$	2.226	62.1%	-3.0%
	$n_s = 2$	2.032	64.5%	-0.6%
	$n_s = 3$	1.926	65.7%	0.6%
	$n_s = 4$	1.913	65.5%	0.4%
hybrid scheme	$n_s = 0$	1.949	65.1%	-
	$n_s = 1$	2.138	62.8%	-2.3%
	$n_s = 2$	1.971	64.6%	-0.5%
	$n_s = 3$	1.936	65.2%	0.1%
	$n_s = 4$	1.884	65.5%	0.4%

size, we utilize the mixed precision training [46] optimization, which uses 16-bit instead of 32-bit floating-point numbers for computation during the training stage. Table IX depicts the training parameters.

Table X shows the final training results. As observed from the results, the accuracy improves as more small-batch workers are introduced with both the dual batch size learning and hybrid methods. In addition, when the number of small-batch workers is not sufficient (e.g., less than or equal to half), the accuracy is lower than the baseline method (all large-batch workers). However, when we increase the number of small-batch workers to more than two, both methods achieve similar performance with the baseline.

On the other hand, the training efficiency is significantly enhanced with the hybrid scheme. The dual batch size learning scheme takes 33,975 seconds to train on ImageNet, while

the hybrid scheme requires only 22,161 seconds, reducing the training time by 35.8%. We also observe that the hybrid scheme achieves significant training time reduction on ImageNet compared to the training on CIFAR-100 (11.1%). This is due to the size ratio between the small-resolution and large-resolution images. The size ratio is 0.31 ( $160^2/288^2$ ) on ImageNet but is 0.56 ( $24^2/32^2$ ) on CIFAR-100. As a result, the hybrid scheme trains the model using relatively smaller images from the training dataset, thus leading to better training efficiency.

### C. Selection of Maximum Batch Size

Selecting an appropriate batch size is crucial in deep learning training, as it directly impacts GPU utilization, training efficiency, and overall performance. Our distributed training schemes begin by selecting the large-batch size ( $B_L$ ), and then determine the small-batch size ( $B_S$ ) through the configuration of the number of small- and large-batch workers ( $n_S$  and  $n_L$ ), based on Equations 4 to 8. In these schemes, the large-batch size ( $B_L$ ) should be as large as possible to fully utilize GPU resources and minimize training time. Hence, the key question is how to determine  $B_L$  before applying our schemes. A typical approach employed by most practitioners is through trial and error, gradually increasing the batch size until the training frameworks (e.g., PyTorch and TensorFlow) trigger a GPU out-of-memory error. To address this issue, we present a method to automate finding  $B_L$  based on linear regression by profiling memory usage, without introducing significant computational overhead.

Assuming that the memory usage scales linearly with batch size  $B$ , we can estimate the total memory usage  $M(B)$  required for training using Equation 9:

$$M(B) = \sum_{l=1}^L p_l + B \times \sum_{l=1}^L a_l \quad (9)$$

where  $p_l$  represents the memory required for the parameters (weights, gradients, etc.) of the  $l$ -th layer,  $a_l$  denotes the memory required for storing and computing the activations per sample at the  $l$ -th layer, and  $L$  is the total number of layers.

Our goal is to determine the maximum batch size  $B_{max}$  such that  $M(B_{max}) \leq M_{GPU}$ , where  $M_{GPU}$  represents the total GPU memory. To achieve this, we run a few batches of different sizes, measure their memory usages, and derive the memory usage model  $M(B)$  using linear regression. This model then allows us to estimate the maximum batch size  $B_{max}$  for the given GPU memory  $M_{GPU}$ .

To verify the prediction accuracy of the derived memory usage model, we conduct experiments on the NVIDIA RTX 3090 GPU with 24 GB of on-device memory, and select eight batches of different sizes (64, 128, 192, 256, 320, 384, 448, 512) for linear regression. Figure 13 shows the measured and predicted maximum memory usage for the CIFAR-100 and ImageNet datasets. For ImageNet, we use mixed precision training, as in Section V-B3. We obtain the maximum batch size of 11,147 for CIFAR-100 with an image resolution of  $32 \times 32$  and 1,345 for ImageNet with an image resolution of  $224 \times 224$ . The corresponding relative error between the

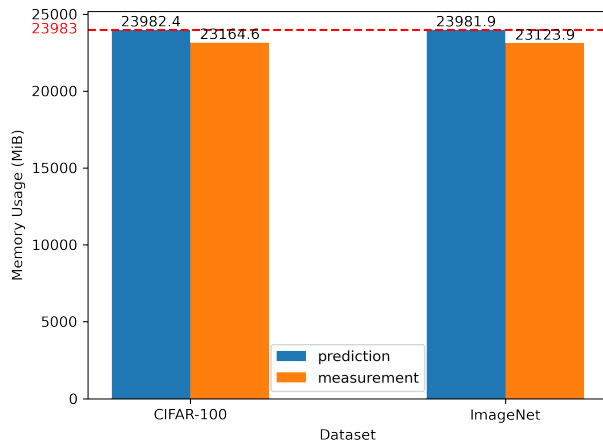


Fig. 13. Comparison of the measured and predicted memory usage for training ResNet-18 on an NVIDIA RTX 3090 GPU. The predicted maximum batch size is 11,147 for image resolution of  $32 \times 32$  on CIFAR-100 and 1,345 for image resolution of  $224 \times 224$  on ImageNet.

predicted and measured values is approximately 3.5% on CIFAR-100 and 3.7% on ImageNet. We conclude that this method is feasible and reliable for our dual batch size learning and hybrid learning schemes.

## VI. CONCLUSION

In this paper, we introduce *dual batch size learning*, a scheme that uses two different batch sizes to co-train a deep neural network. By allowing a small increase in training time, we achieve improved model generalization compared to using a single batch size. To further reduce the training time, we propose *cyclic progressive learning*, which schedules the training process by adjusting image resolution and regularization. Combining these two methods, we present the *hybrid scheme*, which reduces training time while maintaining strong generalization ability by dynamically adjusting both batch sizes and image resolutions during training. In our experiments, the hybrid scheme demonstrates significant time reduction and comparable accuracy when compared to dual batch size learning.

## REFERENCES

- [1] A. Krizhevsky, I. Sutskever, and G. E. Hinton, "Imagenet classification with deep convolutional neural networks," *Commun. ACM*, vol. 60, no. 6, p. 84–90, 2017.
- [2] K. Simonyan and A. Zisserman, "Very deep convolutional networks for large-scale image recognition," 2015.
- [3] K. He, X. Zhang, S. Ren, and J. Sun, "Deep residual learning for image recognition," in *2016 IEEE Conference on Computer Vision and Pattern Recognition (CVPR)*, pp. 770–778, 2016.
- [4] S. Ren, K. He, R. Girshick, and J. Sun, "Faster r-cnn: Towards real-time object detection with region proposal networks," *IEEE Transactions on Pattern Analysis and Machine Intelligence*, vol. 39, no. 6, pp. 1137–1149, 2017.
- [5] W. Liu, D. Anguelov, D. Erhan, C. Szegedy, S. Reed, C.-Y. Fu, and A. C. Berg, "Ssd: Single shot multibox detector," in *Computer Vision – ECCV 2016*, pp. 21–37, 2016.
- [6] J. Redmon, S. Divvala, R. Girshick, and A. Farhadi, "You only look once: Unified, real-time object detection," in *2016 IEEE Conference on Computer Vision and Pattern Recognition (CVPR)*, pp. 779–788, 2016.

- [7] E. Shelhamer, J. Long, and T. Darrell, "Fully convolutional networks for semantic segmentation," *IEEE Transactions on Pattern Analysis and Machine Intelligence*, vol. 39, no. 4, pp. 640–651, 2017.
- [8] L.-C. Chen, G. Papandreou, I. Kokkinos, K. Murphy, and A. L. Yuille, "Deeplab: Semantic image segmentation with deep convolutional nets, atrous convolution, and fully connected crfs," *IEEE Transactions on Pattern Analysis and Machine Intelligence*, vol. 40, no. 4, pp. 834–848, 2018.
- [9] A. Howard, M. Sandler, B. Chen, W. Wang, L.-C. Chen, M. Tan, G. Chu, V. Vasudevan, Y. Zhu, R. Pang, H. Adam, and Q. Le, "Searching for mobilenetv3," in *2019 IEEE/CVF International Conference on Computer Vision (ICCV)*, pp. 1314–1324, 2019.
- [10] T. Ben-Nun and T. Hoefler, "Demystifying parallel and distributed deep learning: An in-depth concurrency analysis," *ACM Comput. Surv.*, vol. 52, no. 4, 2019.
- [11] J. Verbraeken, M. Wolting, J. Katzy, J. Kloppenburg, T. Verbelen, and J. S. Rellermeier, "A survey on distributed machine learning," *ACM Comput. Surv.*, vol. 53, no. 2, 2020.
- [12] S. Shi, Z. Tang, X. Chu, C. Liu, W. Wang, and B. Li, "A quantitative survey of communication optimizations in distributed deep learning," *IEEE Network*, vol. 35, no. 3, pp. 230–237, 2021.
- [13] P. Goyal, P. Dollár, R. Girshick, P. Noordhuis, L. Wesolowski, A. Kyrola, A. Tulloch, Y. Jia, and K. He, "Accurate, large minibatch sgd: Training imagenet in 1 hour," 2018.
- [14] S. L. Smith, P.-J. Kindermans, and Q. V. Le, "Don't decay the learning rate, increase the batch size," in *International Conference on Learning Representations*, 2018.
- [15] Z. Hu, J. Xiao, Z. Tian, X. Zhang, H. Zhu, C. Yao, N. Sun, and G. Tan, "A variable batch size strategy for large scale distributed dnn training," in *2019 IEEE Intl Conf on Parallel & Distributed Processing with Applications, Big Data & Cloud Computing, Sustainable Computing & Communications, Social Computing & Networking (ISPA/BDCLOUD/SocialCom/SustainCom)*, pp. 476–485, 2019.
- [16] N. S. Keskar, D. Mudigere, J. Nocedal, M. Smelyanskiy, and P. T. P. Tang, "On large-batch training for deep learning: Generalization gap and sharp minima," in *International Conference on Learning Representations*, 2017.
- [17] K.-W. Lu, P. Liu, D.-Y. Hong, and J.-J. Wu, "Efficient dual batch size deep learning for distributed parameter server systems," in *2022 IEEE 46th Annual Computers, Software, and Applications Conference (COMPSAC)*, pp. 630–639, 2022.
- [18] S. Hochreiter and J. Schmidhuber, "Flat minima," *Neural Computation*, vol. 9, no. 1, pp. 1–42, 1997.
- [19] A. Krizhevsky, "One weird trick for parallelizing convolutional neural networks," 2014.
- [20] P. Yin, P. Luo, and T. Nakamura, "Small batch or large batch? gaussian walk with rebound can teach," in *Proceedings of the 23rd ACM SIGKDD International Conference on Knowledge Discovery and Data Mining, KDD '17*, p. 1275–1284, 2017.
- [21] T. Takase, S. Oyama, and M. Kurihara, "Why does large batch training result in poor generalization? a comprehensive explanation and a better strategy from the viewpoint of stochastic optimization," *Neural Computation*, vol. 30, no. 7, pp. 2005–2023, 2018.
- [22] T. Takase, "Dynamic batch size tuning based on stopping criterion for neural network training," *Neurocomputing*, vol. 429, pp. 1–11, 2021.
- [23] H. Touvron, A. Vedaldi, M. Douze, and H. Jegou, "Fixing the train-test resolution discrepancy," in *Advances in Neural Information Processing Systems*, vol. 32, 2019.
- [24] A. Brock, S. De, S. L. Smith, and K. Simonyan, "High-performance large-scale image recognition without normalization," in *Proceedings of the 38th International Conference on Machine Learning*, vol. 139 of *Proceedings of Machine Learning Research*, pp. 1059–1071, 2021.
- [25] A. Smola and S. Narayanamurthy, "An architecture for parallel topic models," *Proc. VLDB Endow.*, vol. 3, no. 1–2, p. 703–710, 2010.
- [26] R. Power and J. Li, "Piccolo: Building fast, distributed programs with partitioned tables," in *9th USENIX Symposium on Operating Systems Design and Implementation, OSDI 2010, October 4-6, 2010, Vancouver, BC, Canada, Proceedings*, pp. 293–306, 2010.
- [27] A. Ahmed, M. Aly, J. Gonzalez, S. Narayanamurthy, and A. J. Smola, "Scalable inference in latent variable models," in *Proceedings of the Fifth ACM International Conference on Web Search and Data Mining, WSDM '12*, p. 123–132, 2012.
- [28] M. Li, D. G. Andersen, J. W. Park, A. J. Smola, A. Ahmed, V. Josifovski, J. Long, E. J. Shekita, and B.-Y. Su, "Scaling distributed machine learning with the parameter server," in *11th USENIX Symposium on Operating Systems Design and Implementation (OSDI 14)*, pp. 583–598, 2014.

- [29] M. Li, D. G. Andersen, A. J. Smola, and K. Yu, "Communication efficient distributed machine learning with the parameter server," in *Advances in Neural Information Processing Systems*, vol. 27, 2014.
- [30] A. Gerbessiotis and L. Valiant, "Direct bulk-synchronous parallel algorithms," *Journal of Parallel and Distributed Computing*, vol. 22, no. 2, pp. 251–267, 1994.
- [31] J. Chen, X. Pan, R. Monga, S. Bengio, and R. Jozefowicz, "Revisiting distributed synchronous sgd," 2017.
- [32] B. Recht, C. Re, S. Wright, and F. Niu, "Hogwild!: A lock-free approach to parallelizing stochastic gradient descent," in *Advances in Neural Information Processing Systems*, vol. 24, 2011.
- [33] J. Dean, G. Corrado, R. Monga, K. Chen, M. Devin, M. Mao, M. Ranzato, A. Senior, P. Tucker, K. Yang, Q. Le, and A. Ng, "Large scale distributed deep networks," in *Advances in Neural Information Processing Systems*, vol. 25, 2012.
- [34] T. Chilimbi, Y. Suzue, J. Apacible, and K. Kalyanaraman, "Project adam: Building an efficient and scalable deep learning training system," in *11th USENIX Symposium on Operating Systems Design and Implementation (OSDI 14)*, pp. 571–582, 2014.
- [35] Q. Ho, J. Cipar, H. Cui, S. Lee, J. K. Kim, P. B. Gibbons, G. A. Gibson, G. Ganger, and E. P. Xing, "More effective distributed ml via a stale synchronous parallel parameter server," in *Advances in Neural Information Processing Systems*, vol. 26, 2013.
- [36] H. Cui, J. Cipar, Q. Ho, J. K. Kim, S. Lee, A. Kumar, J. Wei, W. Dai, G. R. Ganger, P. B. Gibbons, G. A. Gibson, and E. P. Xing, "Exploiting bounded staleness to speed up big data analytics," in *2014 USENIX Annual Technical Conference (USENIX ATC 14)*, pp. 37–48, 2014.
- [37] C. Zhang, H. Tian, W. Wang, and F. Yan, "Stay fresh: Speculative synchronization for fast distributed machine learning," in *2018 IEEE 38th International Conference on Distributed Computing Systems (ICDCS)*, pp. 99–109, 2018.
- [38] X. Zhao, A. An, J. Liu, and B. X. Chen, "Dynamic stale synchronous parallel distributed training for deep learning," in *2019 IEEE 39th International Conference on Distributed Computing Systems (ICDCS)*, pp. 1507–1517, 2019.
- [39] A. Paszke, S. Gross, F. Massa, A. Lerer, J. Bradbury, G. Chanan, T. Killeen, Z. Lin, N. Gimelshein, L. Antiga, A. Desmaison, A. Kopf, E. Yang, Z. DeVito, M. Raison, A. Tejani, S. Chilamkurthy, B. Steiner, L. Fang, J. Bai, and S. Chintala, "Pytorch: An imperative style, high-performance deep learning library," in *Advances in Neural Information Processing Systems*, vol. 32, 2019.
- [40] M. Abadi, P. Barham, J. Chen, Z. Chen, A. Davis, J. Dean, M. Devin, S. Ghemawat, G. Irving, M. Isard, M. Kudlur, J. Levenberg, R. Monga, S. Moore, D. G. Murray, B. Steiner, P. Tucker, V. Vasudevan, P. Warden, M. Wicke, Y. Yu, and X. Zheng, "TensorFlow: A system for Large-Scale machine learning," in *12th USENIX Symposium on Operating Systems Design and Implementation (OSDI 16)*, pp. 265–283, 2016.
- [41] S. Chetlur, C. Woolley, P. Vandermersch, J. Cohen, J. Tran, B. Catanzaro, and E. Shelhamer, "cudnn: Efficient primitives for deep learning," 2014.
- [42] M. Tan and Q. Le, "Efficientnetv2: Smaller models and faster training," in *Proceedings of the 38th International Conference on Machine Learning*, vol. 139 of *Proceedings of Machine Learning Research*, pp. 10096–10106, 2021.
- [43] J. Howard, "Training imagenet in 3 hours for usd 25; and cifar10 for usd 0.26," tech. rep., fast.ai, 2018.
- [44] A. Krizhevsky, "Learning multiple layers of features from tiny images," Master's thesis, University of Toronto, 2009.
- [45] O. Russakovsky, J. Deng, H. Su, J. Krause, S. Satheesh, S. Ma, Z. Huang, A. Karpathy, A. Khosla, M. Bernstein, A. C. Berg, and L. Fei-Fei, "Imagenet large scale visual recognition challenge," *International Journal of Computer Vision*, 2015.
- [46] P. Micikevicius, S. Narang, J. Alben, G. Diamos, E. Elsen, D. Garcia, B. Ginsburg, M. Houston, O. Kuchaiev, G. Venkatesh, and H. Wu, "Mixed precision training," in *International Conference on Learning Representations*, 2018.